Edinburgh Research Explorer

Three-Dimensional Spatially Constrained Sulfur Isotopes Highlight Processes Controlling Sulfur Cycling in the Near Surface of the Iheya North Hydrothermal System, Okinawa Trough

OPEN ACCESS

Three-Dimensional Spatially Constrained Sulfur Isotopes Highlight Processes Controlling Sulfur Cycling in the Near Surface of the Iheya North Hydrothermal System, Okinawa Trough

C. LaFlamme[1,2] , S. P. Hollis[3,4] , J. W. Jamieson[5] , and M. L. Fiorentini[1]

[1]Centre for Exploration Targeting, ARC Centre of Excellence in Core to Crust Fluid Systems, School of Earth Sciences, University of Western Australia, Perth, Western Australia, Australia, [2]Département de géologie et de génie géologique, Université Laval, Laval, Québec, Canada, [3]iCRAG (Irish Centre for Research in Applied Geosciences) and School of Earth Sciences, University College Dublin, Dublin, Ireland, [4]Geological Survey Ireland, Dublin, Ireland, [5]Department of Earth Sciences, Memorial University of Newfoundland, St. John's, Newfoundland, Canada

Abstract Modern seafloor hydrothermal systems are unique environments in which many of the Earth's reservoirs, including the hydrosphere, biosphere, and geosphere, dynamically interact. Analysis of spatially constrained sulfur isotope compositions from fluids and hydrothermal precipitates within the discharge zone of a volcanogenic system can be used to trace the interactions between the various isotopically distinct sulfur reservoirs that result in the formation of hydrothermal massive sulfide deposits. Here we present in situ sulfur isotope results from laterally and vertically constrained euhedral hydrothermal pyrite from the Iheya North hydrothermal system in the Okinawa Trough, which was investigated during the Integrated Ocean Drilling Program Expedition 331. Hydrothermal pyrite at the North Big Chimney yields $\delta^{34}S$ values of ~+11.9 ± 1.1‰ (1σ), which are near identical to the $\delta^{34}S$ composition of the vent fluid. Outward, ~150 and ~450 m from North Big Chimney, hydrothermal pyrite within drill core yields $\delta^{34}S$ equal to +10.9 ± 1.3‰ (1σ) and +7.0 ± 3.8‰ (1σ), respectively, showing a shift in isotopic composition away from the main vent site. This evolution to a lighter and more scattered isotopic signature of hydrothermal pyrite (which is easily identifiable from biogenic pyrite) is interpreted to indicate that the hydrothermal fluid leached sulfides (formed previously by biogenic processes) from the surrounding sedimentary strata. As the most significant metal enrichments (Fe, Zn, Cu, Bi, Tl, and Cd) are associated with samples that contain average hydrothermal pyrite $\delta^{34}S$ values similar to $\delta^{34}S$ of the vent fluid, we demonstrate that sulfur isotopes can vector toward metals in seafloor massive sulfide deposits.

1. Introduction

Seafloor hydrothermal systems provide an important mechanism for the transfer of sulfur between seawater, marine sediments, and oceanic crust. The sulfur content of submarine hydrothermal fluids in arc environments is controlled by the interplay of magmatic volatiles (H_2S and/or SO_2), leaching of sulfide minerals from surrounding crust, and thermochemical reduction of seawater sulfate (SO_4^{2-}; Hannington et al., 2005). Mixing and/or fractionation of these sulfur-bearing reservoirs occurs throughout the entire circulating hydrothermal cell and ultimately results in the precipitation of metal sulfides at and below the seafloor. At the sites of hydrothermal discharge, interactions with different local sulfur reservoirs include thermochemical and/or bacterial sulfate reduction of locally entrained seawater sulfate (e.g., Aoyama et al., 2014; McDermott et al., 2015; Ono et al., 2007); leaching of local, near surface reduced sulfur from surrounding crust (McDermott et al., 2015; Ono et al., 2007); and/or adiabatic mixing with seawater (Gilhooly et al., 2014). With the world's first deep-sea mining experiment having occurred in the Okinawa Trough in 2017 (Japan's Ministry of Economy, Trade and Industry, 2017), it has become critical to understand the spatial controls on metal precipitation in active hydrothermal systems as well as the interaction of metal carrying fluids with the biosphere (Van Dover et al., 2017).

Sulfur isotope ratios (measured as $\delta^{34}S = (\frac{\frac{34S}{32S}sample}{\frac{34S}{32S}standard} - 1) \times 1,000$) have been used extensively to investigate the geochemical reservoirs from which sulfur is sourced in mid-ocean ridge spreading centers (cf. Hannington et al., 2005, and references therein). Whereas the sulfur isotope composition of dissolved
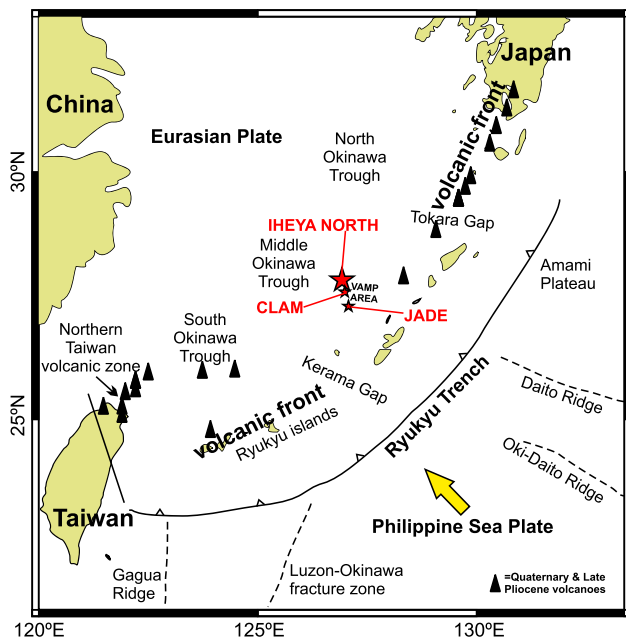
Figure 1. Geological setting of the Iheya North hydrothermal field of the middle Okinawa Trough, Japan (modified after Ishibashi et al., 2015; Shinjo & Kato, 2000). Proximal JADE and CLAM hydrothermal fields also delineated.

H_2S in a modern vent fluid is well constrained to within ±1.0‰ at a given time (e.g., McDermott et al., 2015), $\delta^{34}S$ values of polymetallic sulfides of specific systems can range up to 22‰ (Hannington et al., 2005, and referenced therein). This agrees with $\delta^{34}S$ values of sulfides of the ancient analogues from seafloor massive sulfide systems, volcanogenic massive sulfide (VMS) deposits, which also have reported $\delta^{34}S$ ranges of up to 15‰ (e.g., Ducktown; LeHurray, 1984; Bathurst; Goodfellow & Peter, 1999; Ming; Brueckner et al., 2015; Sullivan; Taylor & Beaudoin, 2000; DeGrussa, Hawke et al., 2015). Rather than precipitating metal sulfide minerals with the same isotopic composition of the vent fluid throughout the entire hydrothermal system, these studies demonstrate that the spatial distribution of sulfur isotope compositions of sulfide minerals vary widely, reflecting time-integrated interactions of sulfur reservoirs and changes in fluid chemistry throughout the system (e.g., Alt et al., 1993; de Ronde et al., 2005).

This study aims to use the spatial distribution of $\delta^{34}S$ values of hydrothermal precipitates from the active Iheya North hydrothermal system, located within the sedimented Okinawa Trough back-arc basin, Japan. We investigate the sulfur isotope evolution of hydrothermal fluids in the shallow subsurface beneath and proximal to an active vent complex, to better understand the processes that control the interplay between sulfur-bearing reservoirs that result in metal sulfide precipitation at and below the seafloor. We present an in situ data set of $\delta^{34}S$ values for euhedral hydrothermal pyrite that is spatially constrained in all three dimensions using samples obtained from drill core at the North Big Chimney (NBC) hydrothermal mound and drill sites several hundreds of meters away, drilled as part of the Integrated Ocean Drilling Program Expedition (IODP) Expedition 331. By comparing the sulfur isotope compositions to mass gain of metals in the sedimented back-arc setting, we improve targeting rationale of metals on the seafloor as well as highlight interaction between hydrothermal fluid and the biosphere outward from a vent. This is important in understanding the genesis of economically important VMS deposits that form in the sedimented back-arc setting, for which there are sparse modern hydrothermal analogues. Additionally, fluid-sediment interactions in seafloor hydrothermal systems are important processes in global biogeochemical budgets but are often difficult to observe and quantify.

2. Geological Setting

The Okinawa Trough extends for ~1,200 km between the Ryukyu arc-trench system and the Eurasian continent (Figure 1). It is interpreted as an incipient intracontinental back-arc basin, still in an early rifting stage prior to seafloor spreading (Shinjo & Kato, 2000). The Iheya North hydrothermal field is located within the middle Okinawa Trough, at ~1,000 m below sea level, ~170 km west of Okinawa, within Japan's exclusive economic zone. It is one of three known hydrothermal fields associated with the subduction of the WNW-ENE trending Daito Ridge (Sibuet et al., 1998). The local stratigraphy is characterized by a rift-related bimodal basaltic-rhyolitic suite of volcanic rocks, accompanied by minor intermediate rocks (Ishizuka et al., 1990; Shinjo & Kato, 2000), and overlain by organic-rich terrigenous sediments sourced from the Yangtze and Yellow rivers (Dou et al., 2010; Takai et al., 2012). A detailed review of hydrothermal fields in the Okinawa Trough is presented in Ishibashi et al. (2015).

The Iheya North hydrothermal field is located in the western cove of the Central Valley of the Iheya North Knoll (Kawagucci et al., 2011; Figure 1). The vent field consists primarily of nine hydrothermal mounds that are aligned north to south. The NBC represents the largest of such structures and is located in the center of the field, venting fluids with a maximum recorded temperature of 311°C (Ishibashi et al., 2015; Nakagawa et al., 2005). During September 2010, IODP Expedition 331 drilled five sites across the Iheya North hydrothermal field, at the NBC mound and 100 to 1,600 m away, to understand the changes in surface expression of the hydrothermal system (see Figure 2). Hydrothermal alteration and mineralization are hosted
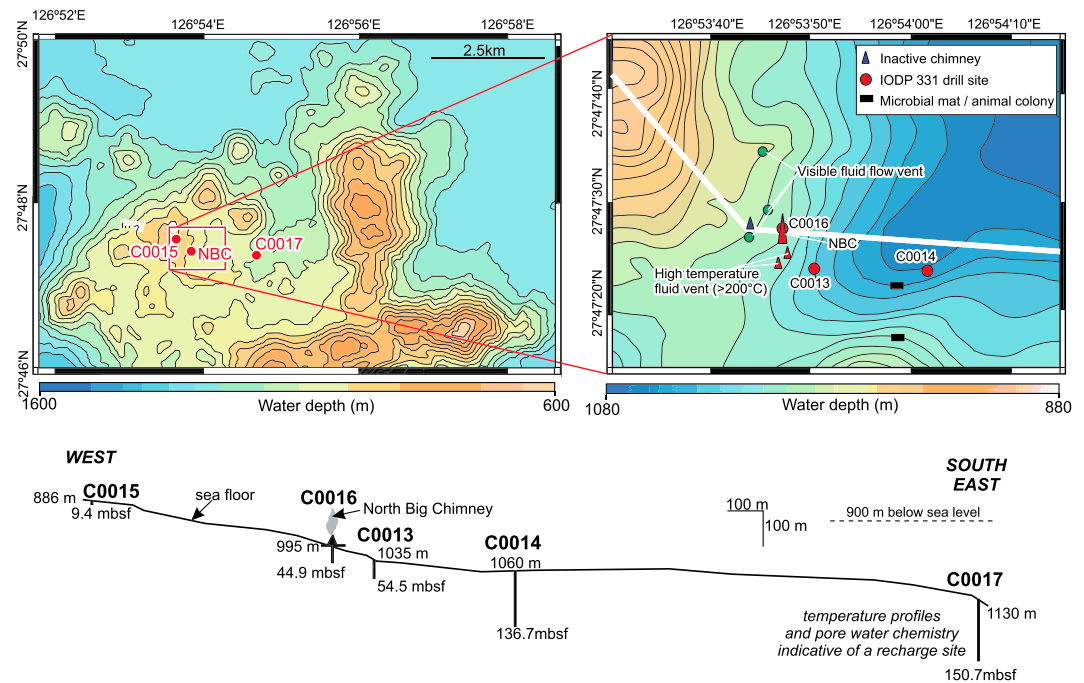
Figure 2. Bathymetric maps of the Iheya North hydrothermal field and Integrated Ocean Drilling Program Expedition 331 drill sites (after Ishibashi et al., 2015; Takai et al., 2011). NBC, North Big Chimney. Schematic cross section of the Iheya North hydrothermal field for the white line delineated in inset.

in a mixed sequence of coarse pumiceous volcaniclastic and fine hemipelagic sediments that overlie a dacitic to rhyolitic volcanic substrate.

Coring adjacent to the foot of the actively venting NBC mound (site C0016 drilled to 45 below seafloor, mbsf) intersected sulfide mineralization that strongly resembles the black ore of the Miocene-age Kuroko VMS deposits of Japan (Takai et al., 2011; Takai et al., 2012). Sphalerite-rich massive sulfides were recovered (metal contents of 30.2% Zn, 12.3% Pb, 2.68% Cu, 33.1-ppm Ag, and 0.07-ppm Au) together with the underlying felsic volcanic rocks that exhibit quartz-muscovite/illite and quartz-Mg-chlorite alteration, similar to footwall alteration associated with Kuroko-type VMS deposits (Yeats et al., 2017). With increasing distance from NBC, the other hydrothermal mounds within the vent field have lower measured vent fluid temperatures and estimated fluid fluxes (Kawagucci et al., 2011).

At site C0013, which occurs ~100 m east of NBC and was drilled to 55 mbsf, surficial coarse-grained sulfidic sediments were recovered with metal contents of 43.2% Zn, 4.4% Pb, 5.4% Cu, 42-ppm Ag, and 0.02-ppm Au (Yeats et al., 2017). Near-surface hydrothermal alteration is dominated by kaolinite and muscovite with locally native sulfur, indicative of acidic hydrothermal fluids (Takai et al., 2012; Figure 3). Below 5 mbsf, the alteration grades to Mg chlorite-dominated assemblages (Takai et al., 2012; Figure 3). Late coarse-grained anhydrite veining overprints earlier alteration and is interpreted to have precipitated from infiltrating seawater as hydrothermal activity waned (Yeats et al., 2017).

Farther east, at site C0014 (~450 m east of NBC, drilled to 137 mbsf), hydrothermal assemblages are characterized by illite/montmorillonite, with Mg-chlorite present at depths below ~30 mbsf (Figure 3). Anhydrite and pyrite are much less abundant than at sites C0016 and C0013, consistent with hydrothermal assemblages typical of distal portions to ancient VMS deposits (Yeats et al., 2017). Located the farthest from NBC (~1.6 km east), site C0017 was drilled to 151 mbsf. The anomalously low heat flow measured at this site, together with concave downward temperature profiles (Takai et al., 2011), and absence of hydrothermal alteration (Yeats et al., 2017), are indicative of a site where oxygenated seawater is infiltrated through layers of coarse-grained pumiceous gravels and breccias. Approximately 600 m northwest of NBC (opposite direction from the other drill sites), site C0015 (drilled to 9 mbsf) is considered to be a background site that is largely unaffected by the hydrothermal system.
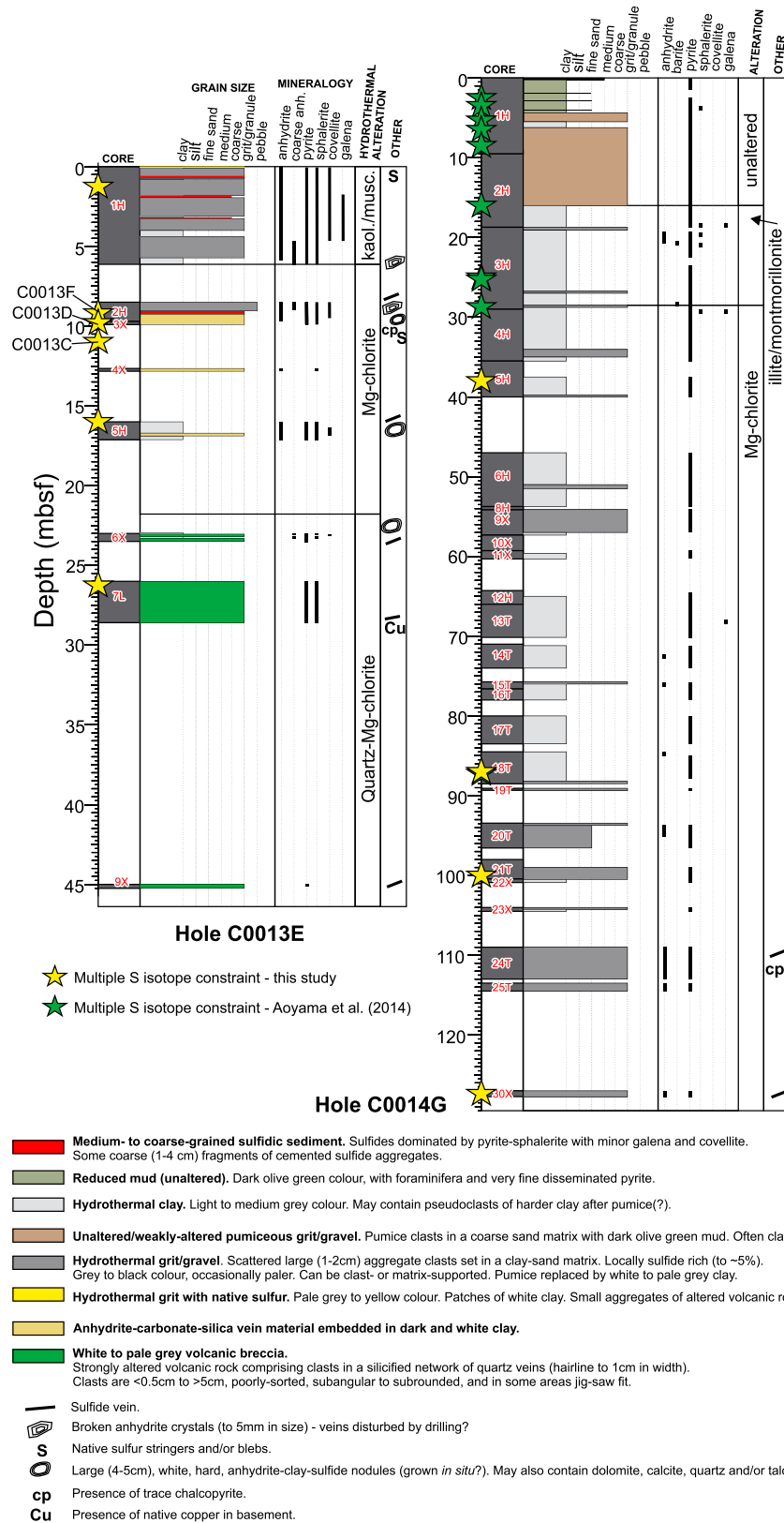
Figure 3. Drill logs demonstrating lithological, alteration, and sampling information pertaining to C0013E and C0014G from Yeats et al. (2017).
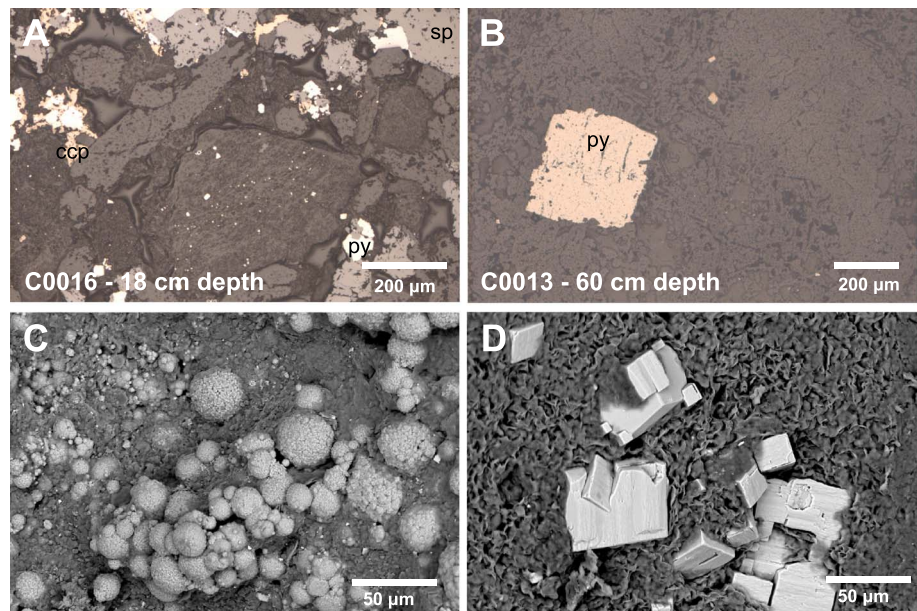
Figure 4. Examples of pyrite textures from Iheya North. Reflected light photomicrographs of massive sulfide in C0016 at 18-cm depth showing intergrown sulfide sphalerite (sp), chalcopyrite (ccp), and pyrite (py) hosted in sericite altered fragments of (a) volcanic glass and (b) euhedral pyrite in volcanic glass. Shipboard backscatter electron images of (c) framboidal pyrite and (d) euhedral hydrothermal pyrite in the uppermost sediments from site C0013 at 1.4-m depth.

Based on observed mineralization, host units, and alteration assemblages, the sediment-rich Iheya North field is interpreted to be an evolving Kuroko-type hydrothermal system (Takai et al., 2011; Yeats et al., 2017), which agrees with the analogy interpreted for the Okinawa Trough by Halbach et al. (1989). The sites drilled during the IODP Expedition 331 provide a discrete profile through this active system (Figure 2). This data set provides a unique opportunity to assess the architectural and geological controls on fluid composition through spatially controlled sulfur isotope analysis of hydrothermal pyrite collected from subsurface core and surface grab samples.

3. Material and Methods

Fourteen samples from sites C0016, C0014, and C0013 that were previously analyzed for whole rock geochemistry (Yeats et al., 2017) were selected for sulfur isotope (^{32}S, ^{33}S, and ^{34}S) analysis. Shipboard scanning electron microscope (SEM) images of drilled rocks and sediments (Figure 4) were acquired using a GEOL 5770 SEM equipped with a backscatter and energy dispersive detectors operating at an accelerating voltage of 15 kV (Yeats et al., 2017). Sediments were rinsed with deionized water in Petri dishes, and euhedral pyrite grains were picked under a binocular microscope. Euhedral pyrite grains (~50 to 100 μm in diameter) were set in the inner 10 mm of a 25-mm diameter epoxy mount. Backscatter images of the picked pyrite grains were acquired using a Tescan Vega-3 SEM at the Centre for Microscopy, Characterization and Analysis, University of Western Australia, for identification of fractures, inclusions, and compositional zoning within the pyrite grains.

Multiple sulfur isotope ratios were determined using a CAMECA IMS1280 large-geometry ion microprobe (SIMS) located Centre for Microscopy, Characterization and Analysis, University of Western Australia using a spot size for analysis was 15 μm. Measurements followed the procedures defined in LaFlamme et al. (2016). Reference material Sierra pyrite (δ^{34}S = 2.1‰, Δ^{33}S = −0.02‰; LaFlamme et al., 2016) was used to correct for drift, monitor internal sample repeatability, and calibrate isotope ratios. Secondary reference material Isua pyrite (δ^{34}S = 4.3‰, Δ^{33}S = +3.1‰; Whitehouse, 2013) was used to monitor the accuracy of the data. All δ^{34}S values are reported using the V-CDT scale (Ding et al., 2001). Values for Δ^{33}S are calculated using a λ value of 0.515 following the equation

Table 1
Summary of Multiple Sulfur Isotope Results from this Study

				$\delta^{34}S$ (‰)						$\Delta^{33}S$ (‰)	
Site	Area	Sample #	Analysis #	Mean	SD	Median	Min.	Max.	Outlier	Mean	SD
C0016	NBC	4	41	11.87	1.05	12.20	9.05	13.49	2	0.03	0.08
C0013	~150 m from NBC	7	55	10.92	1.32	11.45	7.11	12.89	0	0.01	0.09
C0014	~450 m from NBC	4	35	7.03	3.85	7.85	−4.35	11.93	0	0.01	0.07

$$\Delta^{33}S = \delta^{33}S - \left[\left(\delta^{34}S/1000 + 1 \right)^{0.515} - 1 \right] \times 1000$$

to approximate average terrestrial mass-dependent fractionation processes (Farquhar & Wing, 2003). SIMS measurement reproducibility for Sierra pyrite is denoted as twice the standard deviation on the mean of all historical analyses, and the reproducibility on Sierra is $\delta^{34}S = 0.25$‰, $\Delta^{33}S = 0.08$‰ (LaFlamme et al., 2016). Uncertainties (2σ) on measurements reported in the Supplementary Material are ~±0.25‰ for $\delta^{34}S$ and ~±0.17‰ for $\Delta^{33}S$, which takes into account the internal error on the raw isotopic ratios, the uncertainty on the drift correction where necessary and the uncertainty on the standard measurement, calculated as the standard deviation on the mean isotopic ratios measured in the standards. Further details pertaining to analytical parameters, procedures, and calculation of measurement uncertainty are presented in the Supplementary Materials.

4. Results

Pyrite cubes were selected for analysis because they are interpreted to be of hydrothermal origin. We deliberately avoided analyzing local biogenic (i.e., non euhedral hydrothermal) pyrite that occurs in the most unaltered samples and preserves a framboidal texture. Figure 4 demonstrates examples of different pyrite textures. Sulfur isotope compositions from 133 euhedral pyrite spot analyses are summarized in Table 1 (see Supplementary Materials for full results). Uncertainty is reported at one standard deviation on the mean of the total analyses. In most grains, only one measurement was acquired. In certain grains two measurements were made for the center and rim of a euhedral pyrite cube, and in general, grains with multiple measurements, yielded values of $\delta^{34}S$ of within 1.0‰.

Results from site C0016 yield $\delta^{34}S$ values that range from +9.1‰ to +13.5‰ with two outliers with values of +2.2‰ and +5.8‰. These values are similar to $\delta^{34}S$ values for vent fluid H_2S from NBC (+11.2‰ to +12.6‰) reported in Aoyama et al. (2014). Results from site C0013, ~100 m east of NBC, range from +7.1‰ to +12.9‰ and are marginally more dispersed, relative to site C0016. Pyrite from site C0014 contains $\delta^{34}S$ values that range from −4.4‰ to +11.9‰ and show the greatest variability in $\delta^{34}S$ relative to sites C0013 and C0016, including the only measured strongly negative $\delta^{34}S$ values. Isotopically light grains preserve neither distinctive zoning nor features. All $\Delta^{33}S$ values measured in this study are within the measurement analytical uncertainty of 0 ± 0.15‰.

The presented data are complemented by results from Aoyama et al. (2014), who report $\delta^{34}S$ values for pore water sulfate from sites C0014 ($n = 36$) and C0017 ($n = 10$), seawater sulfate, vent fluids from the NBC ($n = 3$), and sulfide-bearing core samples from NBC ($n = 2$), C0014 ($n = 10$, most from <30 mbsf), and surface sediments ($n = 4$). These data are compiled in Figure 5 and presented in the Supplementary Materials.

5. Discussion

The solubility of metals in hydrothermal fluids is controlled by the physical and chemical nature (T, P, pH, redox state, and alkalinity) of the fluid (Hannington, 2014). In hydrothermal seafloor systems the precipitation of metals is generally attributed to mixing of the hydrothermal fluid with cold seawater. However, the chemistry of the ore-forming fluid can change in the near surface environment due to various near-surface processes, such as microbial activity or interaction with sediments. Here we investigate these changes by monitoring the spatial variation in the sulfur isotope composition of pyrite, precipitating from the hydrothermal fluid.
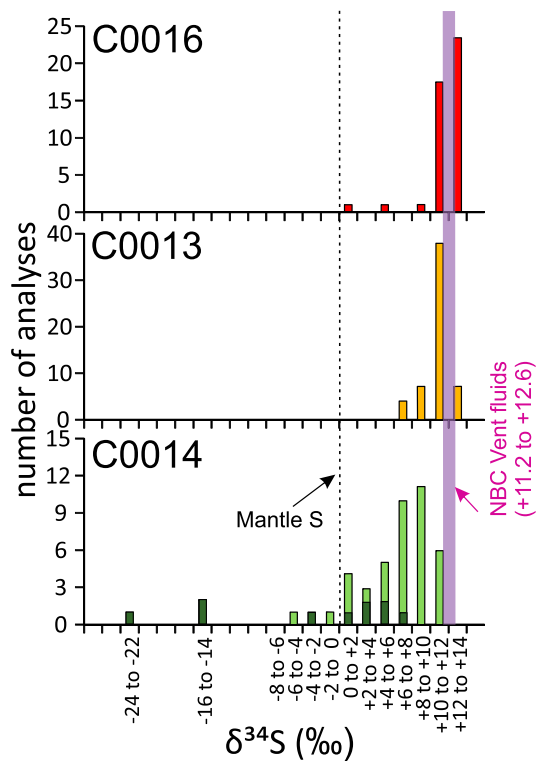
Figure 5. Pyrite $\delta^{34}S$ values from each drill hole: C0016 (NBC hydrothermal mound), C0013 (~100 m from NBC mound), and C0014 (~450 m from NBC mound). Site C0014 includes data from Aoyama et al. (2014) in darker green.

Surface samples from the NBC cluster contain euhedral pyrite that yield $\delta^{34}S$ values near the values measured for the vent fluid ($\delta^{34}S = +11.2‰$ to $+12.6‰$; Aoyama et al., 2014). This indicates that the sulfur reservoir for NBC chimney pyrite is sourced directly from the fluid from which it precipitated and does not include significant contribution from external reduced sulfur sources, since the equilibrium fractionation between H_2S and FeS_2 at hydrothermal conditions (i.e., greater than ~200°C) is less than 2‰ (Ohmoto & Rye, 1979). The shift to increasingly light sulfur isotope compositions away from the discharge site is therefore interpreted to reflect the influence of external sulfur sources, resulting from mixing and/or chemical or biological processes between the hydrothermal fluid and surrounding shallow subsurface environment.

5.1. Spatial Distribution of Alteration Assemblages and $\delta^{34}S$ Values

The sediment and volcanic substrate within the hydrothermal system at Iheya North contains three different alteration mineral assemblages (Figure 6).

At depths greater than 5 mbsf at C0013 (~100 m from NBC mound) and 40 mbsf at C0014 (~450 m from NBC mound), Takai et al. (2011) recognized, using shipboard pore water chemistry data and downhole temperature constraints, a lower zone interpreted as an end-member hydrothermal fluid reservoir based on high fluid K concentrations and very low fluid Mg and SO_4 concentrations (Figure 7; Takai et al., 2011; Aoyama et al., 2014; Yeats et al., 2017). This zone is characterized by Mg-chlorite alteration and the presence of anhydrite. The transition zone between the deeper hydrothermal fluid reservoir and a shallow seawater-dominated reservoir at C0014 and C0013 occurs in the mixed hemipelagic sediments and pumiceous volcanoclastic rocks that are characterized by an alteration assemblage of illite/montmorillonite and/or kaolinite/sericite, with intermediate temperatures assemblages (75–125°C) and intermediate concentrations of K, Mg, and SO_4 (Takai et al., 2011). Aoyama et al. (2014) interpreted sulfur isotope ratios at site C0014 to indicate that sulfides in this zone are formed by active microbial reduction of sulfate; site C0013 was not analyzed. The relationship between sulfur isotopic composition and alteration assemblage, determined by X-ray diffraction profiles (Yeats et al., 2017) and selected pore water chemistry (Takai et al., 2011), is summarized in Figure 7.

Our results indicate a shift from an average composition of $+11.9 \pm 2.1‰$ (2σ) at NBC mound (C0016) to progressively lighter average $\delta^{34}S$ of $+10.9 \pm 2.6‰$ at C0013 and $+7.0 \pm 7.7‰$ at C0014 (Figure 5). This isotopic shift is coincident with lower fluid temperatures (from 311 °C at the NBC vent to <250°C at site C0014) and a change in hydrothermal alteration assemblages with distance from the NBC (Yeats et al., 2017). Variation in $\delta^{34}S$ values does not seem to directly correspond to different alteration assemblages, as shown in Figure 8 where the signature of kaolinite/sericite or illite/montmorillonite altered domains is compared with Mg-chlorite ± quartz assemblages. Only, the uppermost zone of unaltered sediments from 0 to 16 mbsf is
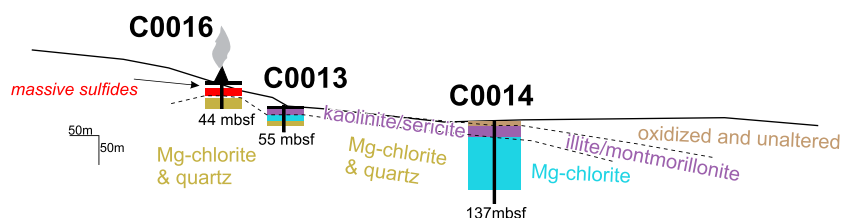

Figure 6. Alteration mineral assemblages (from Yeats et al., 2017) presented in a cross section of drill holes C0016 (NBC mound), C0013 (~100 m from NBC mound), and C0014 (~450 m from NBC mound).
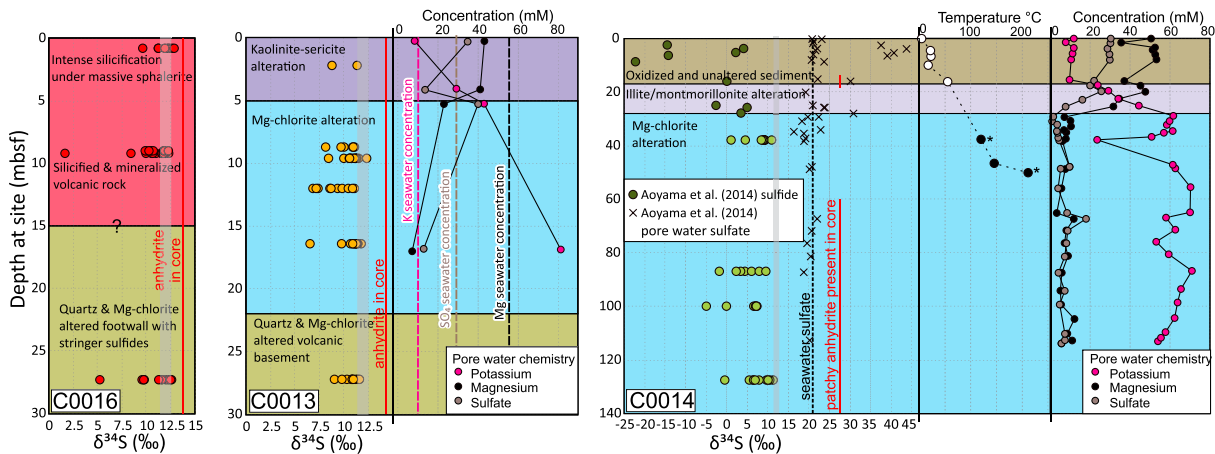
Figure 7. Sulfur isotope data for pyrite from sites C0013 (yellow symbols), C0014 (light green symbols), and C0016 (red symbols) plotted against depth. The δ^{34}S results are plotted with data of sulfides (dark green) and pore water sulfate (x) from Aoyama et al. (2014). The sulfur isotope data are also plotted with alteration assemblages, in situ temperature constraints, and pore water chemistry (from Takai et al., 2011). In situ temperature constraints at site C0014 were measured using an advanced piston corer temperature tool (white circle) and thermoseal strips (black circle), with the latter considered minimum estimates Takai et al., 2011). The red line shows the presence of anhydrite in core, and the gray bar represented vent fluid of Aoyama et al. (2014). Alteration and lithological observations are from Yeats et al. (2017).

marked by a pronounced shift and large spread of δ^{34}S values in pyrite ($-22.2‰$ to $+4.2‰$) and higher δ^{34}S values in pore water sulfate (Aoyama et al., 2014). Further, the uppermost zone is characterized by low temperatures ($<25°C$) and pore water concentrations of Mg, K, and SO_4 close to seawater (Aoyama et al., 2014; Takai et al., 2011; Figure 7).

5.2. Mechanisms Controlling Sulfur Isotope Fractionation

The importance of this section is to highlight mechanisms which can affect the sulfur isotope signature of hydrothermal pyrite in the near-surface rather than the processes that set the isotopic composition of the hydrothermal end-member. Hydrothermal fluids, especially in subduction-related environments, can contain direct input of mantle-sourced sulfur in the form of magmatic degassing of SO_2 and H_2S (Herzig et al., 1998). The hydrothermal fluid can be mixed in the reaction zone with H_2S from reduced seawater sulfate and/or leached sulfide that has been transported to the reaction zone. It can further interact with seawater sulfate and the sulfur-bearing stratigraphy during the upward course of the fluid to surface. This section does not speculate on the interactions between sulfur reservoirs prior to and during mixing in the reaction zone. Rather it investigates the control on the spatial distribution of sulfur isotope signatures of precipitating metal-bearing sulfides in the near-surface, focusing on the reactions that promote phase changes that precipitate sulfides throughout the hydrothermal system.
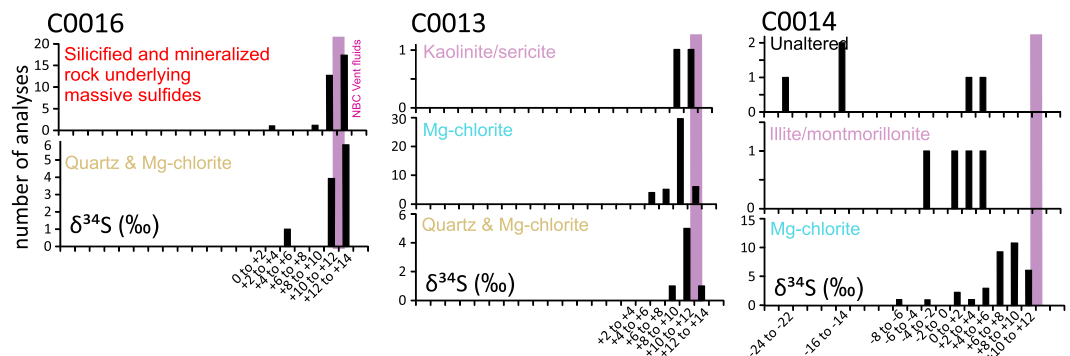

Figure 8. Spatially constrained δ^{34}S results compared to corresponding alteration mineral assemblages of host rocks delineated in Figures 4 and 5. Vent fluid of Aoyama et al. (2014) expressed as a purple line.

5.2.1. Leaching of Sulfur From Surrounding Strata

The uppermost unaltered zone of C0014 is interpreted to represent a fluid reservoir dominated by seawater-derived anoxic pore fluids where primary microbial sulfate reduction is occurring. High precision sulfur isotopes from Aoyama et al. (2014) report that pyrite from unaltered sediments at C0014 yield $\delta^{34}S$ values as low as −24‰, whereas residual pore water sulfate yields $\delta^{34}S$ values up to +30‰. These values are consistent with Rayleigh distillation reactions for bacterial reduction of seawater sulfate (see Seal, 2006). Interaction between hydrothermal fluid and surrounding sulfide-bearing originally unaltered sediments has the potential to shift the H_2S fluid signature to lighter values away from the main vent, as observed in this study.

5.2.2. Thermochemical Reduction of Sulfate

Thermochemical reduction of seawater sulfate can occur through interaction with Fe^{2+} derived from fayalite and/or magnetite at temperatures between 200 and 350°C (Meshoulam et al., 2016, and references therein). Modern seawater sulfate has a $\delta^{34}S$ of +21.0 ± 0.2‰ (Rees et al., 1978). Downwelling seawater driven by hydrothermal circulation may also be a significant source of sulfate-derived reduced sulfur to the subseafloor hydrothermal system (Ono et al., 2007; Shanks, 2001). While dissolved sulfate is largely removed from seawater in the downwelling leg of these circuits, in response to its progressive heating, owing to the retrograde solubility of anhydrite (Bischoff & Seyfried, 1978), any remaining sulfate will be thermochemically reduced deep in the high temperature reaction zone. In addition to downwelling seawater from the recharge zone, seawater entrainment has been recognized by McDermott et al. (2015) within the shallow subsurface upflow zone. The maximum sulfur isotope fractionation by thermochemical reduction is 15‰; however, many of the hydrothermal pyrite grains analyzed in this study yield $\delta^{34}S < 5$‰, which are too light to be fractionated by this mechanism. While it is likely that this process had a role in the isotopic composition of the end-member hydrothermal fluid, measured at the vent to be ~+12‰ (Aoyama et al., 2014), it cannot explain the shift to lighter sulfur isotope values of hydrothermal pyrite away from the venting site.

5.2.3. Disproportionation of Sulfur Dioxide

Low-pH fluids, reflecting disproportionation of SO_2 are common in back-arc seafloor hydrothermal systems (Gamo et al., 1997; Herzig et al., 1998) and may influence crustal alteration and metal mobilization (Herzig et al., 1998). Degassing of SO_2 from silicic magmas can play a critical role in regulating sulfur speciation in hydrothermal systems. Upon cooling of volcanic gases below 300–400°C, SO_2 undergoes hydration and disproportionates according to the reactions $3SO_2 + 2H_2O = 2HSO_4^- + S_0 + 2H^+$ and $4SO_2 + 4H_2O = 3HSO_4^- + H_2S + 3H^+$. Disproportionation of SO_2 is a temperature-dependent equilibrium process that leads to ^{34}S-enriched HSO_4^- and ^{34}S-depleted H_2S relative to the initial SO_2 composition (Herzig et al., 1998; Ohmoto & Rye, 1979). In the near surface, oxidizing environment, the H_2SO_4 dissociates further to produce acids which leach the rocks. This can lead to the formation of characteristic acid-sulfate alteration assemblages (e.g., Herzig et al., 1998). While this mechanism is likely occurring near the surface, based on the high temperatures and acidic assemblages described in section 2, it cannot be responsible for a lateral shift to lighter sulfur isotope values in the near surface. This is because we would not expect the processes to be amplified at lower temperatures away from the NBC vent.

5.2.4. Bacterial Reduction of Seawater Sulfate

In the subseafloor environment, sulfate can be reduced through microbial pathways by the equation $2(CH_2O) + SO_4^{2-} \rightarrow H_2S + 2HCO_3^-$. During this process, isotopically light sulfate is preferentially reduced, resulting in sulfur products with a negative $\delta^{34}S$ signature (Canfield, 2001; Seal, 2006; Thode et al., 1961). This mechanism has been proposed in the formation of the Palinuro massive sulfide complex in the Tyrrhenian Sea in Italy, based on the multiple sulfur isotope signature of core samples (up to 5 m depth) within the hydrothermal system (Peters et al., 2011).

Despite a concentrated effort to characterize the microbial communities across the Iheya North hydrothermal field, microorganisms linked to sulfate reduction have not been detected in the majority of rocks and sediments (Kawagucci et al., 2013; Takai et al., 2011, 2012; Zhang et al., 2015). According to Muyzer and Stams (2008), sulfate reducing microorganisms can be grouped into seven phylogenetic lineages—five within Bacteria (*Deltaproteobacteria*, *Nitrospirae*, *Clostridia*, *Thermodesulfobiaceae*, and *Thermodesulfobacteria*) and two within Archea (*Eurarchaeota* and *Crenarchaeota*). Only three of these lineages (*Nitrospirae*, *Thermodesulfobacteria*, and *Thermodesulfobiaceae*) contain thermophilic sulfate reducers (Muyzer & Stams, 2008). The lack of amplified DNA for samples collected from sites C0016 and C0013

demonstrates that detectable microbial communities were not well developed (Kawagucci et al., 2013). This is a consequence of the high temperatures (>150°C) and acidic nature of the hydrothermal fluids (pH = 4.8–5.4; Kawagucci et al., 2011) being significantly outside the thermochemical optimum growth conditions for thermophilic sulfate reducing bacteria like *Thermodesulfobacteria* (T = 65–75°C; pH = 6.0–7.5; Jeanthon et al., 2002; Kawagucci et al., 2011, 2013; Muyzer & Stams, 2008). In their study of microbes from vent sites of the Middle Valley, Frank et al. (2013) determined maximum rates of sulfate reduction occurred at 90°C at all three sites with the microbial community dominated by the thermophilic *Thermodesulfovibrio*. Microorganisms such as *Epsilonproteobacteria* and many others that are dominant in microbial habitats associated with hydrothermal vent fluids and chimney structures (Zhang et al., 2015) may locally have a role in carbon and sulfur cycling (e.g., sulfur oxidation; Muyzer & Stams, 2008), but they are not involved in sulfate reduction (Campbell et al., 2006).

Aoyama et al. (2014) demonstrate that isotopically light pyrite in the unaltered zone of C0014 were formed by bacterial reduction of seawater sulfate. However, the underlying zones beneath the unaltered zone at C0014 form euhedral grains of hydrothermal pyrite which preserve an overall lighter sulfur isotope signature than the main vent. Aside from the sulfides formed by bacterial reduction of seawater sulfate in the unaltered zone as presented in Aoyama et al. (2014), the hydrothermal pyrite grains elsewhere in the system were not formed by this mechanism, and the overall shift to a lighter isotopic signature is interpreted to occur by leaching of pyrite from the surrounding strata.

5.3. Interaction Between Hydrothermal Fluid and Surrounding Benthic Strata

The chemically conservative Δ^{33}S tracer can be used to investigate interactions between the discharging hydrothermal fluid and the sedimentary cover in seafloor systems (Ono et al., 2007; Peters et al., 2011). Positive Δ^{33}S values are preserved in sulfides formed by microbial seawater sulfate reduction (Farquhar et al., 2003; Johnston, 2011, and references therein). Therefore, in hydrothermal systems, positive Δ^{33}S values have been interpreted to indicate either mixing and incorporation of reduced sedimentary sulfur with the hydrothermal fluid (e.g., McDermott et al., 2015; Ono et al., 2007) or the involvement of bacterial seawater sulfate reduction in the formation of massive sulfides (Peters et al., 2011). Using bulk high precision analytical techniques, Aoyama et al. (2014) investigated the δ^{34}S and Δ^{33}S signature vent sulfides and fluids and the most unaltered surface sediments (to a depth of 87 m) and pore water sulfate (to a depth of 108 m) at C0014. At or near the surface at C0014, surface sedimentary sulfides yield δ^{34}S $\approx$ −20‰ to −10‰ and Δ^{33}S = +0.06‰. This signature is consistent with their formation from bacterial reduction of seawater sulfate (δ^{34}S = +21.2‰ and Δ^{33}S = +0.05‰; Rees et al., 1978; Tostevin et al., 2014) coinciding with residual pore water sulfate with δ^{34}S = up to +30‰ and Δ^{33}S = up to +0.08‰ (Aoyama et al., 2014).

In situ SIMS analysis of sulfur isotopes yields a precision that is an order of magnitude less than high precision bulk methods, resulting in the inability to resolve small values of and small shifts in Δ^{33}S. The results here demonstrate that all samples yield Δ^{33}S = 0.02 ± 0.16‰ (2SD on the mean), which is an order of magnitude too large in precision to discern the positive Δ^{33}S values discussed above. Nevertheless, in situ analyses provide a means to rapidly understand the δ^{34}S architecture of a system. The isotopic composition of individual hydrothermal pyrite grains throughout the hydrothermal systems represents the sum of all subsurface chemical exchange processes that occur from recharge to discharge. By analyzing δ^{34}S of spatially distributed surface and subsurface samples, results from this study provide insight into the significant fluid-substrate interactions that take place in the immediate surroundings to a vent before discharge.

The trend toward lighter δ^{34}S values away from the hydrothermal vent indicates an increased component of an isotopically light sulfur reservoir. Aoyama et al. (2014) demonstrate that in the unaltered sediments forming the top layer of C0014, bacterial seawater sulfate reduction is occurring to form isotopically light diagenetic pyrite with a small positive Δ^{33}S value. However, the sulfur isotope architecture of the system presented here indicates that deeper in this section and throughout C0016 and C0013 pyrite previously formed by this process is being leached into hydrothermal fluids and altering the surrounding strata to form pyrite-bearing hydrothermal sediments (Figure 9). While the elevated temperatures prevented the occurrence of bacteria at C0013 and below ~30 m at C0014, heat promoted the rapid leaching reaction H_2S + FeS (Rickard, 1997; Rickard & Luther, 1997). It is, however, important to note that isotopic
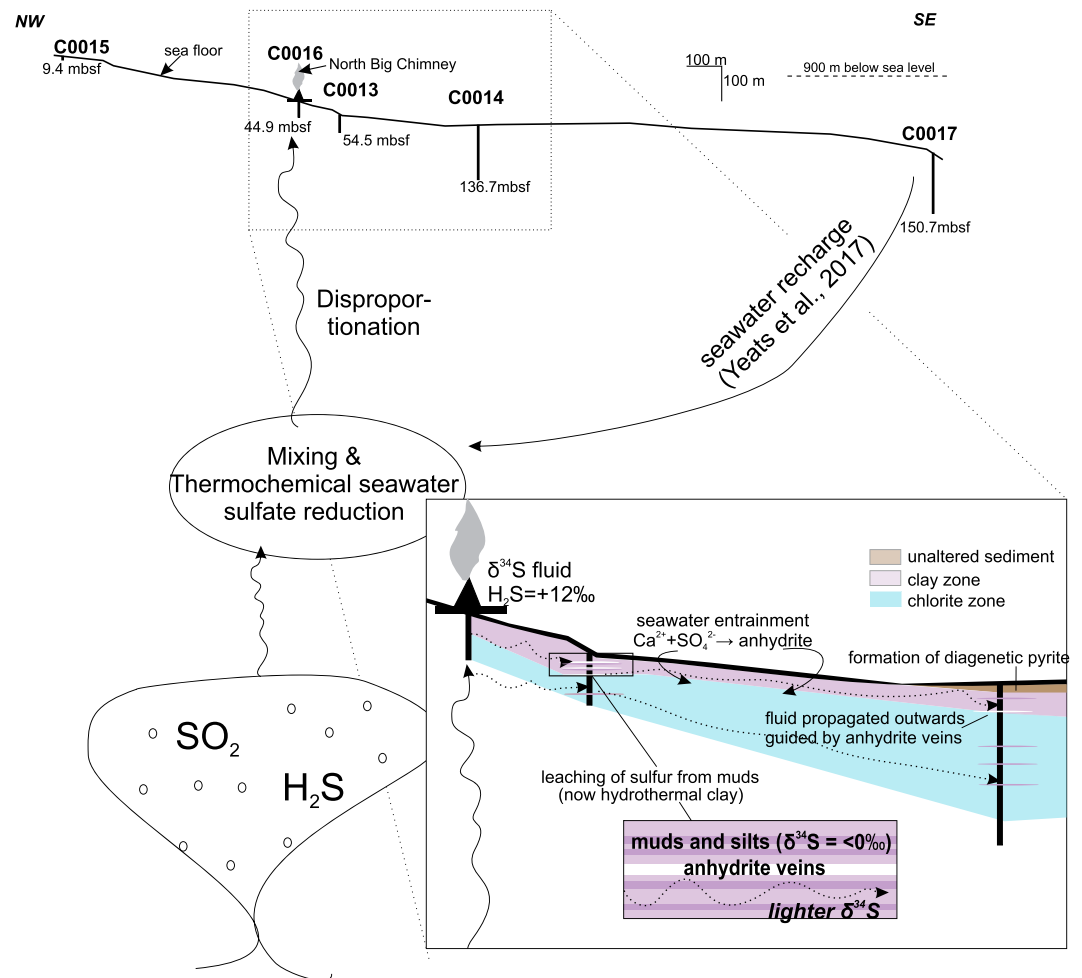
Figure 9. Schematic model determined by spatially monitoring $\delta^{34}S$ values lateral and at depth to the North Big Chimney of the Iheya North seafloor hydrothermal system. Larger scale cycling of reservoirs is modified after McDermott et al. (2015). Inset demonstrates increased interaction between hydrothermal fluid and surrounding strata away from the NBC resulting in increasingly lighter $\delta^{34}S$.

fractionation of FeS-H$_2$S is not temperature dependent (Ohmoto & Rye, 1979); therefore, $\delta^{34}S$ values are a product of mixing between two reservoir sources. Precipitation of pyrite from the hydrothermal fluid occurred in the near surface following cooling of the fluid. Here we interpret that leaching of sulfides previously formed by microbial sulfate reduction into the hydrothermal fluid away from the vent results in the precipitation of pyrite with increasingly lighter $\delta^{34}S$ values, rather than bacterial sulfate reduction as the cause of metal sulfide precipitation. The observation that crustal host rock is an important sulfur reservoir in these systems is consistent with the observations at other spreading centers including at mid-ocean ridges (Mid Atlantic Ridge, East Pacific Rise, and Guaymas Basin) and back-arc ridges (Eastern Manus Basin and Lau Basin; McDermott et al., 2015; Ono et al., 2007). The interaction of the metalliferous hydrothermal fluid and the surrounding strata is important to our understanding of metal precipitation in a hydrothermal system as we attempt to grasp the environmental considerations, such as disruption of the subsurface biosphere, of deep-sea mining (Sharma, 2017; Van Dover et al., 2017).

5.4. Relationship of Sulfur Isotopes to Metal Contents

Many of the largest VMS deposits preserved in the rock record formed in sedimented back-arc environments (e.g., Galley et al., 2007; Piercey, 2009). Classic examples include VMS deposits of the Iberian Pyrite Belt and the Bathurst Mining Camp, Canada (Galley et al., 2007). Sediments can act to trap and insulate metals before they can escape into the water column (Hannington et al., 2005). In preserved volcano-sedimentary terranes,
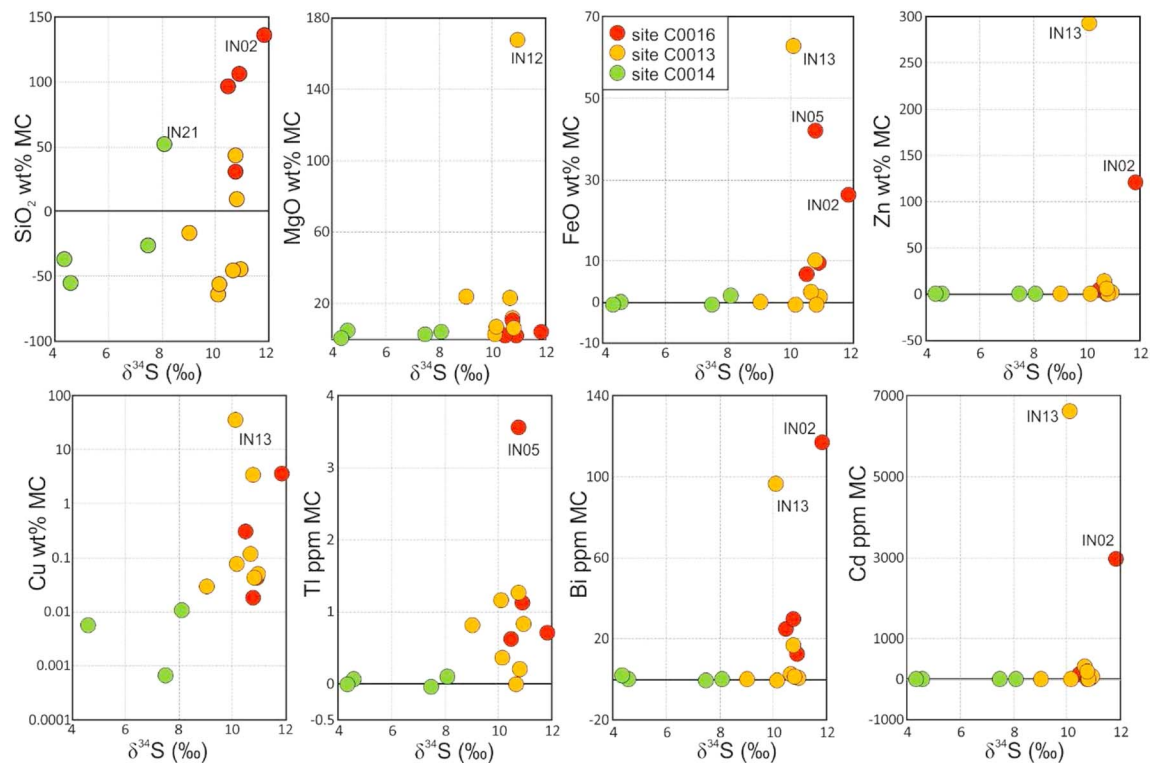
Figure 10. Calculated whole rock mass change values plotted against mean $\delta^{34}S$ values for samples from sites C0016, C0013, and C0014. Samples which yielded strongly negative sulfur isotope values of Aoyama et al. (2014) are not included here as we do not have whole rock geochemical data for these rocks. However, as strongly negative $\delta^{34}S$ values are restricted to unaltered sediments, mass gains of the above elements should be effectively zero. Plotted on a log-scale to better visualize data.

VMS exploration is difficult, relying on the recognition of a favorable host stratigraphy (Hollis et al., 2015) and the identification of zones of hydrothermal discharge through alteration mineralogy and lithogeochemistry (Piercey, 2009).

Here we compare spatially controlled sulfur isotope data to the lithogeochemical results collected from the same samples and presented in Yeats et al. (2017) to aid exploration for VMS deposits forming in sedimented back-arcs. In ancient VMS and modern seafloor sulfide systems, most elements including Si, Mg, Fe, Ca, the LILE, and transition metals are readily mobilized by hydrothermal fluids (see Piercey, 2009). Exceptions typically include Al, the high field strength elements (HFSE; Ti, Zr, Hf, and Y), and REE (minus Eu; Piercey, 2009). Mass balance equations compare altered rocks to their unaltered equivalents using mass transfer equations and ratios of elements demonstrated to remain immobile during hydrothermal alteration (Barrett & MacLean, 1994; Grant, 1986). The principle aim is to quantify the amounts of individual elements added to and subtracted from the rock, as significant mass change anomalies may not be apparent in untreated data due to the effects of closure (Barrett & MacLean, 1994). Several approaches exist to estimate mass transfers in VMS systems, including the isocon method (e.g., Grant, 1986), use of Pearce element ratios (Stanley & Madeisky, 1996), and immobile element techniques. Mass change values here were calculated using the single precursor method of Barrett and MacLean (1994), with Zr as the immobile element monitor.

Absolute mass change for each component is calculated according to: $\Delta^a = [Z^o/Z^a . C^a] - C^o$, where Δ^a is the absolute mass change expressed in g/100 g; C^o is the wt % proportion of the mobile component in the altered rock; C^a is the wt % proportion of the mobile component in the precursor; Z^o is the proportion of the immobile element in the precursor; Z^a is the proportion of the immobile element in the altered rock. Sample IN07, a gray woody pumice from distal site C0017, was used as a precursor composition after Yeats et al. (2017), which displays identical immobile element ratios to pumiceous sediments at sites C0013, C0014, and C0016 and felsic rock samples from the underlying basement (Figure 3; Yeats et al., 2017).

Calculated mass change values for Si, Fe, Mg, Cu, Bi, and Tl show systematic relationships to average δ^{34}S values with increased values toward NBC mound (Figure 10). Larger mass gains of Fe, Cu, Zn, Cd, Bi, and Tl toward the hydrothermal mound (site C0016) are to be expected, given our current understanding of hydrothermal alteration associated with VMS systems (reviewed in Piercey, 2009). Whereas Zn and Pb sulfides are associated with massive sulfides, Cu and Fe sulfides typically dominate in underlying feeder zones. Cadmium will be preferentially incorporated into sphalerite. Thallium halos have been recognized proximal to sedimented back-arc VMS deposits (Large et al., 2001), with the most significant enrichments here again associated with strongly positive δ^{34}S values (Figure 9). As the most significant metal enrichments in this system are associated with δ^{34}S values above +10‰, this may be used as a vector to mineralization within the seafloor hydrothermal system. Elevated MgO and SiO$_2$ concentrations at site C0016 (and to a lesser extent at C0013) are a consequence of quartz and Mg-chlorite alteration (e.g., Galley et al., 2007; Piercey, 2009) where hydrothermal fluids are dominant in the feeder zones (Aoyama et al., 2014; Takai et al., 2011). Our data suggest that the recognition of strongly positive δ^{34}S values for pyrite may be used as a proxy for zones of hydrothermal upflow when exploring for VMS deposits in these environments.

6. Conclusions

Here we demonstrate that sulfur isotope architecture in three dimensions of the Iheya North hydrothermal system records interaction between a hydrothermal fluid and the benthic community-hosting sedimentary strata away from the NBC. This interaction is recorded by systematically lighter δ^{34}S values away from the main vent site. Characterizing the interactions between hydrothermal fluids and the near-surface environment as well as the size of seafloor deposits is critical for the technical and environmental considerations surrounding deep-sea mining. Sulfur isotope vectoring may have the potential to aid in this understanding.

References

Alt, J. C., Shanks, W. C. III, & Jackson, M. C. (1993). Cycling of sulfur in subduction zones: The geochemistry of sulfur in the Mariana island arc and backarc trough. *Earth and Planetary Science Letters*, *119*(4), 477–494. https://doi.org/10.1016/0012-821X(93)90057-G

Aoyama, S., Nishizawa, M., Takai, K., & Ueno, Y. (2014). Microbial sulfate reduction within the Iheya North subseafloor hydrothermal system constrained by quadruple sulfur isotopes. *Earth and Planetary Science Letters*, *398*, 113–126. https://doi.org/10.1016/j.epsl.2014.04.039

Barrett, T. J., & MacLean, W. H. (1994). Chemostratigraphy and hydrothermal alteration in exploration for VHMS deposits in greenstones and younger volcanic rocks. In D. R. Lentz (Ed.), *Alteration and alteration processes associated with ore-forming systems*, *Short Course Notes, 11* (pp. 433–467). St. John's, NL: Geological Association of Canada.

Bischoff, J. L., & Seyfried, W. E. (1978). Hydrothermal chemistry of seawater from 25°C to 350°C. *American Journal of Science*, *278*(6), 838–860. https://doi.org/10.2475/ajs.278.6.838

Brueckner, S., Piercey, S., Layne, G., Piercey, G., & Sylvester, P. (2015). Variations of sulphur isotope signatures in sulphides from the metamorphosed Ming Cu(−Au) volcanogenic massive sulphide deposit, Newfoundland Appalachians, Canada. *Mineralium Deposita*, *50*(5), 619–640. https://doi.org/10.1007/s00126-014-0567-7

Campbell, B. J., Engel, A. S., Porter, M. L., & Takai, K. (2006). The versatile ε-proteobacteria: Key players in sulphidic habitats. *Nature Reviews*, *4*(6), 458–468. https://doi.org/10.1038/nrmicro1414

Canfield, D. E. (2001). Biogeochemistry of sulfur isotopes. *Reviews in Mineralogy and Geochemistry*, *43*, 60–636.

De Ronde, C. E. J., Hannington, M. D., Stoffers, P., Wright, I. C., Ditchburn, R. G., Reyes, A. G., et al. (2005). Evolution of a submarine magmatic-hydrothermal system: Brothers volcano, southern Kermadec arc, New Zealand. *Economic Geology*, *100*(6), 1097–1133. https://doi.org/10.2113/gsecongeo.100.6.1097

Ding, T., Valkiers, S., Kipphardt, H., Bievre, P., Taylor, P., Gonfiantini, R., & Krouse, R. (2001). Calibrated sulfur isotope abundance ratios of three IAEA sulfur isotope reference materials and V-CDT with a reassessment of the atomic weight of sulfur. *Geochimica et Cosmochimica Acta*, *65*(15), 2433–2437. https://doi.org/10.1016/S0016-7037(01)00611-1

Dou, Y., Tang, S., Liu, Z., Clift, P. D., Shi, X., & Berne, S. (2010). Provenance discrimination of siliciclastic sediments in the middle Okinawa Trough since 30 ka: Constraints from rare Earth element composition. *Marine Geology*, *275*(1-4), 212–220. https://doi.org/10.1016/j.margeo.2010.06.002

Farquhar, J., Johnston, D., Wing, B., Habicht, K., Canfield, D., Airieau, S., & Thiemens, M. (2003). Multiple sulphur isotopic interpretations of biosynthetic pathways: Implications for biological signatures in the sulphur isotope record. *Geobiology*, *1*(1), 27–36. https://doi.org/10.1046/j.1472-4669.2003.00007.x

Farquhar, J., & Wing, B. A. (2003). Multiple sulfur isotopes and evolution of the atmosphere. *Earth and Planetary Science Letters*, *213*(1-2), 1–13. https://doi.org/10.1016/S0012-821X(03)00296-6

Frank, K. L., Rogers, D. R., Olins, H. C., Vidoudez, C., & Girguis, P. R. (2013). Characterizing the distribution and rates of microbial sulfate reduction at Middle Valley hydrothermal vents. *The ISME Journal*, *7*(7), 1391–1401. https://doi.org/10.1038/ismej.2013.17

Galley, A. G., Hannington, M. D., & Jonasson, I. R. (2007). Volcanogenic massive sulphide deposits. In W. D. Goodfellow (Ed.), *Mineral deposits of Canada: A synthesis of major deposit-types, district metallogeny, the evolution of geological provinces, and exploration methods*, *Special Publication No. 5* (pp. 141–161). St. John's: Geological Association of Canada, Mineral Deposits Division.

Gamo, T., Okamura, K., Charlou, J.-L., Urabe, T., Auzende, J.-M., Ishibashi, J., et al. (1997). Acidic and sulfate-rich hydrothermal fluids from the Manus backarc basin, Papua New Guinea. *Geology*, *25*(2), 139–142. https://doi.org/10.1130/0091-7613(1997)025<0139:AASRHF>2.3.CO;2

Gilhooly, W. P., Fike, D. A., Druschel, G. K., Kafantaris, F.-C. A., Price, R. E., & Amend, J. P. (2014). Sulfur and oxygen isotope insights into sulfur cycling in shallow-sea hydrothermal vents, Milos, Greece. *Geochemical Transactions*, *15*(1), 12. https://doi.org/10.1186/s12932-014-0012-y

Goodfellow, W., & Peter, J. (1999). Sulphur isotope composition of the Brunswick no. 12 massive sulphide deposit, Bathurst Mining Camp, New Brunswick: Implications for ambient environment, sulphur source, and ore genesis. *Canadian Journal of Earth Sciences*, *36*(1), 127–134. https://doi.org/10.1139/e99-031

Grant, J. A. (1986). The isocon diagram—A simple solution to Gresens' equation for metasomatic alteration. *Economic Geology*, *81*(8), 1976–1982. https://doi.org/10.2113/gsecongeo.81.8.1976

Halbach, P., Nakamura, K., Wahsner, M., Lange, J., Sakai, H., Käselitz, L., et al. (1989). Probable modern analogue of Kuroko-type massive sulphide deposits in the Okinawa Trough back-arc basin. *Nature*, *338*(6215), 496–499. https://doi.org/10.1038/338496a0

Hannington, M. D. (2014). 13.18—Volcanogenic massive sulfide deposits. In H. D. Holland & K. K. Turekian (Eds.), *Treatise on geochemistry* (2nd ed., pp. 463–488). Oxford: Elsevier.

Hannington, M. D., de Ronde, C. E. J., & Petersen, S. (2005). Sea-floor tectonics and submarine hydrothermal systems. In J. W. Hedenquist, J. F. H. Thompson, R. J. Goldfarb, & J. P. Richards (Eds.), *Economic geology 100th anniversary volume* (pp. 111–141). Littleton, CO: Society of Economic Geologists.

Hawke, M., Davidson, G., Meffre, S., Large, R. R., Gemmell, B., & Hilliard, P. (2015). *Geological evolution and metal source of the DeGrussa Cu-Au-Ag volcanic-hosted massive sulfide deposit* (pp. 2063–2066). Western Australia Western Australia: Society for geology applied to mineral deposits, Nancy.

Herzig, P. M., Hannington, M. D., & Arribas, A. (1998). Sulfur isotopic composition of hydrothermal precipitates from the Lau backarc: Implications for magmatic contributions to seafloor hydrothermal systems. *Mineralium Deposita*, *33*(3), 226–237. https://doi.org/10.1007/s001260050143

Hollis, S. P., Yeats, C. J., Wyche, S., Barnes, S. J., Ivanic, T. J., Belford, S. M., et al. (2015). A review of volcanic-hosted massive sulfide (VHMS) mineralization in the Archaean Yilgarn craton, Western Australia: Tectonic, stratigraphic and geochemical associations. *Precambrian Research*, *260*, 113–135. https://doi.org/10.1016/j.precamres.2014.11.002

Ishibashi, J.-I., Ikegami, F., Tsuji, T., & Urabe, T. (2015). Hydrothermal activity in the Okinawa Trough backarc basin: geological background and hydrothermal mineralisation. In J.-I. Ishibashi (Ed.), *Subseafloor biosphere linked to hydrothermal systems* (pp. 337–359). Japan: Springer, TAIGA Concept.

Ishizuka, H., Kawanobe, Y., & Sakai, H. (1990). Petrology and geochemistry of volcanic rocks dredged from the Okinawa Trough, an active backarc basin. *Geochemical Journal*, *24*(2), 75–92. https://doi.org/10.2343/geochemj.24.75

Japan's Ministry of Economy, Trade and Industry Press Release (2017). World's first success in continuous ore lifting test for seafloor poly-metallic sulfides. September 26, 2017.

Jeanthon, C., L'Haridon, S., Cueff, V., Banta, A., Reysenbach, A.-L., & Prieur, D. (2002). Thermodesulfobacterium hydrogeniphilum sp. nov., a thermophilic, chemolithoautotrophic, sulfate-reducing bacterium isolated from a deep-sea hydrothermal vent at Guaymas Basin, and emendation of the genus Thermodesulfobacterium. *International Journal of Systematic and Evolutionary Microbiology*, *52*(Pt 3), 765–772. https://doi.org/10.1099/00207713-52-3-765

Johnston, D. T. (2011). Multiple sulfur isotopes and the evolution of Earth's surface sulfur cycle. *Earth-Science Reviews*, *106*(1-2), 161–183. https://doi.org/10.1016/j.earscirev.2011.02.003

Kawagucci, S., Chiba, H., Ishibashi, J.-I., Yamanaka, T., Toki, T., Muramatsu, Y., et al. (2011). Hydrothermal fluid geochemistry at the Iheya North field in the mid-Okinawa Trough: Implication for origin of methane in subseafloor fluid circulation systems. *Geochemical Journal*, *45*(2), 109–124. https://doi.org/10.2343/geochemj.1.0105

Kawagucci, S., Miyazaki, J., Nakajima, R., Nozaki, T., Takaya, Y., Kato, Y., et al. (2013). Post-drilling changes in fluid discharge pattern, mineral deposition, and fluid chemistry in the Iheya North hydrothermal field, Okinawa Trough. *Geochemistry, Geophysics, Geosystems*, *14*, 4774–4790. https://doi.org/10.1002/2013GC004895

LaFlamme, C., Martin, L., Jeon, H., Reddy, S., Selvaraja, V., Caruso, S., et al. (2016). In situ multiple sulfur isotope analysis by SIMS of pyrrhotite, pentlandite and chalcopyrite to refine magmatic ore genetic models. *Chemical Geology*, *444*, 1–15. https://doi.org/10.1016/j.chemgeo.2016.09.032

Large, R. R., McPhie, J., Gemmell, J. B., Herrmann, W., & Davidson, G. J. (2001). The spectrum of ore deposit types, volcanic environments, alteration halos, and related exploration vectors in submarine volcanic successions: Some examples from Australia. *Economic Geology*, *96*(5), 913–938. https://doi.org/10.2113/gsecongeo.96.5.913

LeHurray, A. P. (1984). Lead and sulfur isotopes and a model for the origin of the Ducktown deposit, Tennessee. *Economic Geology*, *79*(7), 1561–1573. https://doi.org/10.2113/gsecongeo.79.7.1561

McDermott, J. M., Ono, S., Tivey, M. K., Seewald, J. S., Shanks, W. C., & Solow, A. R. (2015). Identification of sulfur sources and isotopic equilibria in submarine hot-springs using multiple sulfur isotopes. *Geochimica et Cosmochimica Acta*, *160*, 169–187. https://doi.org/10.1016/j.gca.2015.02.016

Meshoulam, A., Ellis, G. S., Ahmad, W. S., Deev, A., Sessions, A. L., Tang, Y., et al. (2016). Study of thermochemical sulfate reduction mechanism using compound specific sulfur isotope analysis. *Geochimica et Cosmochimica Acta*, *188*, 73–92. https://doi.org/10.1016/j.gca.2016.05.026

Muyzer, G., & Stams, A. J. M. (2008). The ecology and biotechnology of sulphate-reducing bacteria. *Nature Reviews*, *6*(6), 441–454. https://doi.org/10.1038/nrmicro1892

Nakagawa, S., Takai, K., Inagaki, F., Chiba, H., Ishibashi, J., Kataoka, S., et al. (2005). Variability in microbial community and venting chemistry in a sediment-hosted backarc hydrothermal system: Impacts of subseafloor phase-separation. *FEMS Microbiology Ecology*, *54*(1), 141–155. https://doi.org/10.1016/j.femsec.2005.03.007

Ohmoto, H., & Rye, R. O. (1979). Isotopes of sulfur and carbon. In H. L. Barnes (Ed.), *Geochemistry of hydrothermal ore deposits* (2nd ed., pp. 509–567). New York: John Wiley and Sons.

Ono, S., Shanks, W. C. III, Rouxel, O. J., & Rumble, D. (2007). S-33 constraints on the seawater sulfate contribution in modern seafloor hydrothermal vent sulfides. *Geochimica et Cosmochimica Acta*, *71*(5), 1170–1182. https://doi.org/10.1016/j.gca.2006.11.017

Peters, M., Strauss, H., Petersen, S., Kummer, N.-A., & Thomazo, C. (2011). Hydrothermalism in the Tyrrhenian Sea: Inorganic and microbial sulfur cycling as revealed by geochemical and multiple sulfur isotope data. *Chemical Geology*, *280*(1-2), 217–231. https://doi.org/10.1016/j.chemgeo.2010.11.011

Piercey, S. J. (2009). Lithogeochemistry of volcanic rocks associated with volcanogenic massive sulphide deposits and applications to exploration. In B. Cousens & S. J. Piercey (Eds.), *Submarine volcanism and mineralisation: Modern through ancient, Short Course 29–30 May 2008* (pp. 15–40). Canada: Geological Association of Canada.

Rees, C. E., Jenkins, W. J., & Monster, J. (1978). The sulphur isotopic composition of ocean water sulphate. *Geochimica et Cosmochimica Acta*, *42*(4), 377–381. https://doi.org/10.1016/0016-7037(78)90268-5

Rickard, D. (1997). Kinetics of pyrite formation by H2S oxidation of iron (II) monosulfide in aqueous solutions between 25 and 125 C: The rate equation. *Geochimica et Cosmochimica Acta*, *61*(1), 115–134. https://doi.org/10.1016/S0016-7037(96)00321-3

Rickard, D., & Luther, G. W. (1997). Kinetics of pyrite formation by the H_2S oxidation of iron (II) monosulfide in aqueous solutions between 25 and 125°C: The mechanism. *Geochimica et Cosmochimica Acta*, *61*(1), 135–147. https://doi.org/10.1016/S0016-7037(96)00322-5

Seal, R. (2006). Sulfur isotope geochemistry of sulfide minerals. *Sulfide Mineralogy and Geochemistry*, *61*(1), 633–677. https://doi.org/10.2138/rmg.2006.61.12

Shanks, W. C. (2001). Stable isotopes in seafloor hydrothermal systems: Vent fluids, hydrothermal deposits, hydrothermal alteration, and microbial processes. *Reviews in Mineralogy and Geochemistry*, *43*(1), 469–525. https://doi.org/10.2138/gsrmg.43.1.469

Sharma, R. (2017). Deep-sea mining: Current status and future considerations. In R. Sharma (Ed.), *Deep-sea mining: Resource potential, technical and environmental considerations* (Chap. 1, pp. 3–21). Switzerland: Springer.

Shinjo, R., & Kato, Y. (2000). Geochemical constraints on the origin of bimodal magmatism at the Okinawa Trough, an incipient backarc basin. *Lithos*, *54*(3-4), 117–137. https://doi.org/10.1016/S0024-4937(00)00034-7

Sibuet, J.-C., Deffontaines, B., Hsu, S.-K., Thareau, N., Le Formal, J.-P., & Liu, C.-S. (1998). Okinawa Trough backarc basin: Early tectonic and magmatic evolution. *Journal of Geophysical Research*, *103*(B12), 30,245–30,267. https://doi.org/10.1029/98JB01823

Stanley, C. R., & Madeisky, H. E. (1996). *Lithogeochemical exploration for metasomatic zones associated with hydrothermal mineral deposits using Pearce element ratio analysis, University of Bristol short course notes, January 1996* (p. 98). Vancouver, Canada: Mineral Deposit Research Unit.

Takai, K., Mottl, M. J., Nielsen, S. H., & Expedition 331 Scientists (2011). *Proceedings of the IODP, 331*. Washington, DC: Integrated Ocean Drilling Program Management International, Inc, La Jolla, CA.

Takai, K., Mottl, M. J., & Nielsen, S. H. H. (2012). IODP expedition 331: Strong and expansive subseafloor hydrothermal activities in the Okinawa Trough. *Scientific Drilling*, *13*, 19–27. https://doi.org/10.5194/sd-13-19-2012

Taylor, B. E., & Beaudoin, G. (2000). Sulphur stratigraphy of the Sullivan Pb-Zn-ag deposit, BC: Evidence for hydrothermal sulphur, and bacterial and thermochemical sulphate reduction. In J. W. Lydon, T. Hoy, J. F. Slack, & M. Knapp (Eds.), *The Sullivan deposit and its geological environments* (Vol. 1, pp. 696–719). St. John's NL: Special Publication Mineral Deposits Division of the Geological Association of Canada.

Thode, H. G., Monster, J., & Dunford, H. B. (1961). Sulfur isotope geochemistry. *Geochimica et Cosmochimica Acta*, *25*(3), 159–174. https://doi.org/10.1016/0016-7037(61)90074-6

Tostevin, R., Turchyn, A. V., Farquhar, J., Johnston, D. T., Eldridge, D. L., Bishop, J. K. B., & McIlvin, M. (2014). Multiple sulfur isotope constraints on the modern sulfur cycle. *Earth and Planetary Science Letters*, *396*, 14–21. https://doi.org/10.1016/j.epsl.2014.03.057

Van Dover, C. L., Ardon, J. A., Escobar, E., Gianni, M., Gjerde, K. M., Jaeckel, A., et al. (2017). Biodiversity loss from deep-sea mining. *Nature Geoscience*, *10*(7), 464–465. https://doi.org/10.1038/ngeo2983

Whitehouse, M. (2013). Multiple sulfur isotope determination by SIMS: Evaluation of reference sulfides for $\Delta^{33}S$ with observations and a case study on the determination of $\Delta^{36}S$. *Geostandards and Geoanalytical Research*, *37*(1), 19–33. https://doi.org/10.1111/j.1751-908X.2012.00188.x

Yeats, C. J., Hollis, S. P., Halfpenny, A., Corona, J.-C., LaFlamme, C., Southam, G., et al. (2017). Actively forming Kuroko-type volcanic-hosted massive sulfide (VHMS) mineralisation at Iheya North, Okinawa Trough, Japan. *Ore Geology Reviews*, *80*, 20–41.

Zhang, J., Sun, Q.-l., Zeng, Z., Chen, S., & Sun, L. (2015). Microbial diversity in the deep-sea sediments of the Iheya North and Iheya ridge, Okinawa Trough. *Microbiological Research*, *177*, 43–52. https://doi.org/10.1016/j.micres.2015.05.006